Reproductive Biology and Endocrinology

RESEARCH

Open Access

17α-Ethynylestradiol alters testicular epigenetic profiles and histone-to-protamine exchange in mice

L. Ded[1*], E. Zatecka-Lanska[1], E. Vaculikova[1], M. Frolikova[1], O. Sanovec[1], V. Palenikova[1], O. Simonik[1], A. Dorosh[1], H. Margaryan[1], F. Elzeinova[1], A. Kubatova[1], J. Peknicova[1], A. Paradowska-Dogan[3], K. Steger[1] and K. Komrskova[1,2*]

Abstract

Spermatogenesis starts with the onset of puberty within the seminiferous epithelium of the testes. It is a complex process under intricate control of the endocrine system. Physiological regulations by steroid hormones in general and by estrogens in particular are due to their chemical nature prone to be disrupted by exogenous factors acting as endocrine disruptors (EDs). 17α-Ethynylestradiol (EE2) is an environmental pollutant with a confirmed ED activity and a well-known effect on spermatogenesis and chromatin remodeling in haploid germ cells. The aim of our study was to assess possible effects of two doses (2.5ng/ml; 2.5 µg/ml) of EE2 on both histone-to-protamine exchange and epigenetic profiles during spermatogenesis performing a multi/transgenerational study in mice. Our results demonstrated an impaired histone-to-protamine exchange with a significantly higher histone retention in sperm nuclei of exposed animals, when this process was accompanied by the changes of histone post-translational modifications (PTMs) abundancies with a prominent effect on H3K9Ac and partial changes in protamine 1 promoter methylation status. Furthermore, individual changes in molecular phenotypes were partially transmitted to subsequent generations, when no direct trans-generational effect was observed. Finally, the uncovered specific localization of the histone retention in sperm nuclei and their specific PTMs profile after EE2 exposure may indicate an estrogenic effect on sperm motility and early embryonic development via epigenetic mechanisms.

Keywords 17α-Ethynylestradiol, EE2, Endocrine disruptors, Post-translational modifications, Testis, Sperm, Histone-to-protamine exchange, Transgenerational study, DNA methylation

Introduction

Spermatogenesis is a highly specialized physiological process which in mammals takes place in testis from puberty onwards and is under intricate control of the endocrine system [1]. Spermatogonia, which represent male germ stem cells, undergo self-renewal (mitotic divisions) and, on a regular basis, differentiate into primary spermatocytes, which enter meiosis and become secondary spermatocytes (first meiotic division) and round spermatids (second meiotic division). Subsequently, in a process called spermiogenesis, round spermatids differentiate to elongating spermatids and finally to spermatozoa. As a

*Correspondence:
L. Ded
lukas.ded@ibt.cas.cz
K. Komrskova
katerina.komrskova@ibt.cas.cz
[1]Laboratory of Reproductive Biology, Institute of Biotechnology of the Czech Academy of Sciences, BIOCEV, Vestec, Czech Republic
[2]Department of Zoology, Faculty of Science, Charles University, Vinicna 7, Prague 2, Czech Republic
[3]Department of Urology, Pediatric Urology and Andrology, Molecular Andrology, Biomedical Research Center of the Justus-Liebig University, Giessen, Germany

result of the permanent basal-to-luminal differentiation within the seminiferous epithelium, the different germ cell populations (best identifiable by the shape of their nuclei) within the seminiferous tubule arrange in specific stages of so-called spermatogenic cycle. The change of both cellular and nuclear shape is especially prominent during spermiogenesis, when DNA-binding histones are replaced by protamines in the process called histone-to-protamine exchange and the process continues during epididymal maturation [2].

Estrogens are a group of steroid hormones primarily known for their role in the regulation of the female estrous cycle. Estrogens are no longer considered as female-only hormones, as they play a crucial role in the testicular and spermatogenic processes [3–6]. In adult mammals, there are three major estrogen forms (estrone (E1), estradiol (E2), and estriol (E3)) acting both via genomic and non-genomic pathways. Their well-balanced blood levels and tissue abundances and subsequent complex, highly regulated estrogen signaling is vital for the proper spermatogenetic process including chromatin remodeling in spermatids [7]. Both high or low non-physiological estrogen levels or dis-regulated signaling process are then disruptive for testicular function and sperm production [8].

Endocrine disruptors (EDs) are chemical compounds that interfere with the normal function of the endocrine system [9]. This interference includes physiological hormone production, transport and effect in target tissues. Physiological regulations by steroid hormones are due to their chemical nature, which is prone to be disrupted by exogenous factors, when in case of estrogens this disruption can be mediated both by natural (phytoestrogens) and synthetic (xeno)estrogens. One of the major synthetic estrogen is 17α-Ethynylestradiol (EE2), which is widely present in contraceptive pills, as well as used during the treatment of gynecological disorders, hormone sensitive cancers and menopausal symptoms [10, 11]. Since its stable structure resistant for metabolic degradation [12], EE2 is considered as significant environmental pollutant with confirmed negative effect on both human population and wildlife [13, 14].

One of the major concerns related to EDs exposure is their effect on the directly exposed population, and also on its progeny. This effect is known to be multigenerational, in case some cells or tissues (especially reproductive organs and gametes) which are directly exposed to EDs as well as transgenerational, when no tissue type including parental germ cells is directly exposed to the agent [15]. This transgenerational transmission can be conducted by either female or male lineage and/or by both parents. Since EDs usually do not cause a direct genotoxic effect with corresponding changes in the DNA sequence, epigenetic mechanisms are expected to represent the major mechanism of the molecular and subsequent cellular/histological/organismal phenotypes transmittance across generations [16]. Epigenetic events are mediated by multiple molecular mechanisms, which fall into three major molecular changes domains: (1) Histone post-translational modifications (PTMs; also histone marks/signatures); (2) DNA methylation; and (3) RNA-interference. It is of relevance that all three domains were already shown to mediate inter-generational transmittance of the (pathological) phenotypes after EDs exposure [17, 18].

In the present study, we aimed to assess possible effects of 17α-Ethynylestradiol (EE2) on both histone-to-protamine exchange and epigenetic profiles during spermatogenesis. We also aimed to adopt specific cross-breeding strategy for F1 and F2 generations to estimate a potential multi/cumulative/trans-generational effects and their transmittance through the male or female lineage. We hypothesized to find significant differences between control and exposed groups by using antibodies specific for the histone post-translational modifications histone H3 acetylated at lysine residue 9 (H3K9ac), histone H3 tri-methylated at lysine residue 27 (H3K27me3) and histone H3 tri-methylated at lysine residue 36 (H3K36me3). Finally, in addition to histone PTMs analyses, we applied pyrosequencing to study the degree of DNA methylation and its potential role for transmittance of altered molecular phenotypes while focusing on Protamine 1 promotor.

Materials and methods

Antibodies and chemicals

All chemicals were purchased from Sigma-Aldrich; Czechia unless otherwise specified. The antibodies used in the study were purchased from Abcam and their specifications are listed below.

Animals

C57BL/6 inbred mice strain was used in the experiment. Animals were housed in an animal facility (Institute of Molecular Genetics, ASCR, v. v. i.) under standard experimental conditions (constant temperature (23–24 °C), humidity (60±5%) and 12-h light regime) This study was conducted in accordance with the Guide for the Care and use of Laboratory Animals (NIH Publication Eight edition 2011). The experimental protocol was approved by the Animal Care and Use Committee of the Institute of Molecular Genetics ASCR and carried out in accordance with the regular relevant guidelines and regulations (file number 17OZ9715/2019–18134).

EE2 exposure design

17α-Ethynylestradiol (EE2) was administrated in carbon-filtered drinking water ad libitum in two doses emulating the potential environmental dose (D1; 2.5ng/ml),

contraceptive dose (D2; 2.5 µg/ml) and control group (vehicle); $N_{animals} = 5_{min} - 8_{max}$ per control/experimental groups according to the breeding outputs. The exposure of females of F0 generation started at 4th post-partum week and was terminated at 9th week in case of contraceptive dose D2 to avoid EE2 contraceptive effect during breeding, at 10th week, and demonstrate the potential trans-generational effect in F2 generation. Both males and females exposed to environmental dose D1 were exposed continuously. Males of F0 generation were exposed from post-partum 4th week till 10th week when they were mated with F0 females for 6 h overnight in cages without EE2 drinking water. F1 and F2 generations were then produced with respect to study potential paternally or maternally transmitted multi-generational, cumulative, and trans-generational effect of EE2 exposure (Fig. 1). Animals used for analysis were sacrificed at 11th week and reproductive organs including testes and epididymis were collected.

Testicular tissue analysis

Immunohistochemistry staining and imaging

Testicular paraffine sections were deparaffinized using DIASOLV 2×5 min. After paraffine removal, samples were hydrated in decreasing ethanol series (100%, 90%, 70%) for 5 min in each solution followed by rinsing in distilled water and PBS. Antigen retrieval was performed in a pressure cooker for 15 min in 0,1 M citrate buffer pH 6. After, samples were cooled down at the room temperature for 30 min and permeabilized with Intracellular Staining Perm Wash Buffer 3×5 min (BioLegend, USA). Superblock solution (Thermofisher, USA) was applied prior to the primary antibodies for 1 h at room temperature in the humid chamber. Primary antibodies were diluted 1:200 in the Antibody diluent (Zytomed Systems GmbH, Germany) and applied overnight at 4 °C. The next day, samples were washed in PBS 3×5 min at room temperature (RT) with orbital shaking at 100 RPM. Secondary antibodies (AlexaFluor 488, 568, Abcam, GB) were diluted 1:500 in Antibody diluent and applied in a humid chamber for 1 h. Samples were washed 3×10 min, mounted using the Vectashield with DAPI (Vector Laboratories, USA) and sealed with nail polish. Testicular tissue sections were analyzed under Carl Zeiss Zeiss LSM 710 and LSM 880 inverted confocal microscopes and processed using Zen software (Fig. 2A-E).

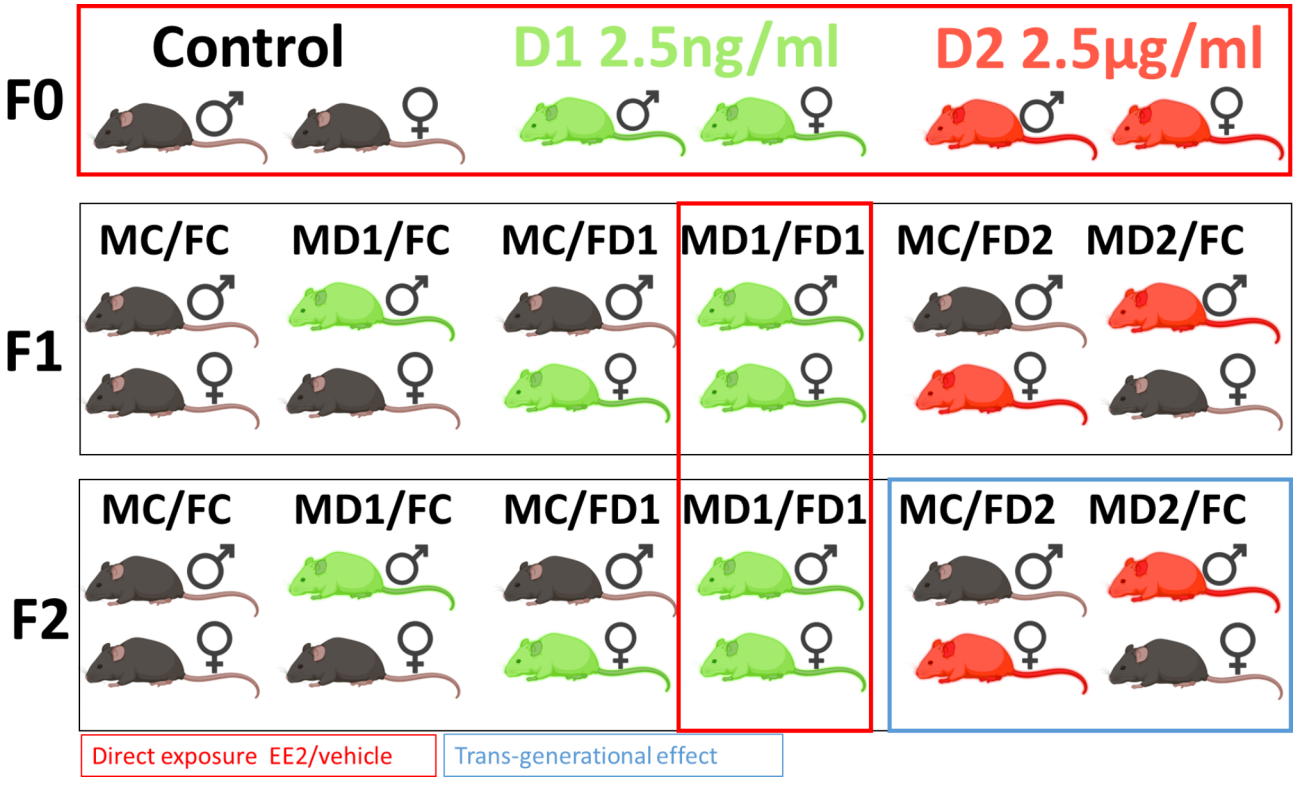

Fig. 1 Scheme showing in vivo exposure and breeding of control and experimental mouse groups in F0 generation to produce F1 and F2 progeny. Animals directly exposed to EE2 doses D1 and D2 are indicated by red rectangles, animals probing the potential trans-generational effect by blue rectangle. MC – male control; FC – female control; MD1 – male from lineage exposed to dose D1; FD1 – female from lineage exposed to dose D1; MD2 – male from lineage exposed to dose D2; FD2 – female from lineage exposed to dose D2

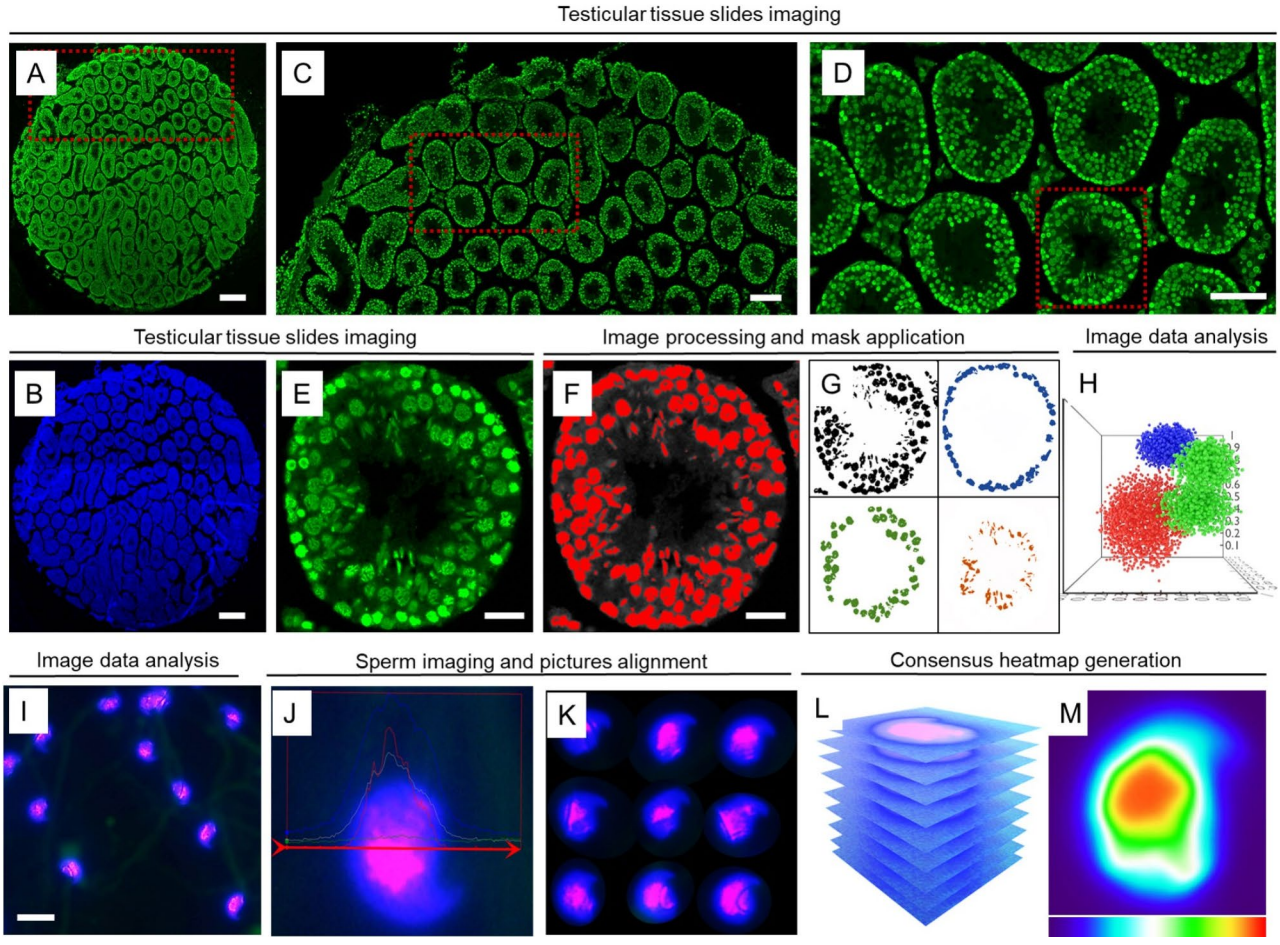

Fig. 2 Testicular tissue slides and epididymal sperm imaging and image analysis. (**A**) Tile scan of the entire testicular tissue section H3 staining; scale bar indicates 300 µm. (**B**) DAPI counter-staining of the corresponding section; scale bar indicates 300 µm. **C**-**D**) Magnification of the region of interest (ROI) of the section; scale bars indicates 200 µm (**C**) and 100 µm (**D**). **E**) Individual seminiferous tubule ROI; scale bar indicates 50 µm. **F**) Application of the mask for individual cell nuclei fluorescent signal isolation; scale bar indicates 50 µm. **G**) Isolation of signals from individual cell populations (black – all cells; blue – spermatogonia; green – spermatocytes; red/orange – spermatids and sperm. **H**-**I**) Visualization of individual cell populations blue – spermatogonia; green – spermatocytes; red/orange – spermatids and sperm in 3D Principal component analysis (PCA) plot (**I**) (see Fig. 3 for details) (**H**). Fluorescent signal of H3 staining (magenta) of decondensed sperm nuclei counter stained with DAPI (blue); scale bar indicates 10 µm (**I**). **J**) Relative fluorescent intensities (RFI) histograms over the sperm head stained with anti-H3 antibody. **K**-**L**) Alignment of fluorescent signals from nuclei (**K**), their super-position (**L**) for consensus heat map generation (**M**)

Table 1 Specifications of the primary antibodies used in the study

Abcam catalogue number	Specificity of the antibody/molecular target
ab6002	Anti-Histone H3 (tri methyl K27) antibody
ab10812	Anti-Histone H3 (acetyl K9) antibody
ab1791	Anti-Histone H3 antibody
ab9050	Anti-Histone H3 (tri methyl K36) antibody

Semi-automatic in situ fluorescent analysis of the histone PTMs in of testicular tissue sections

To assess the relative fluorescent intensities (RFI; and corresponding histones and histone PTMs abundancies) after indirect antibody-staining (primary antibodies specified in Table 1; Alexa Fluor 488/568, anti-mouse/anti-rabbit secondary antibodies, Abcam, GB) of the testicular tissue sections from control and experimental animals, the semiautomatic life image processing platform was utilized. First, the DAPI-positive image elements (cell nuclei) were identified using intensity mask (Fig. 2F) and the lumen centers were semi-manually marked. Then, signals from individual testicular cell populations (Fig. 2G) were isolated using PCA filters based on the cells size, roundness/complexity and distance from lumen (Figs. 2H and 3). The proper identification of individual cell populations by mask-based PCA filter was controlled by experienced histologist (LD) during the life image acquisition (400x). The collected RFI of the

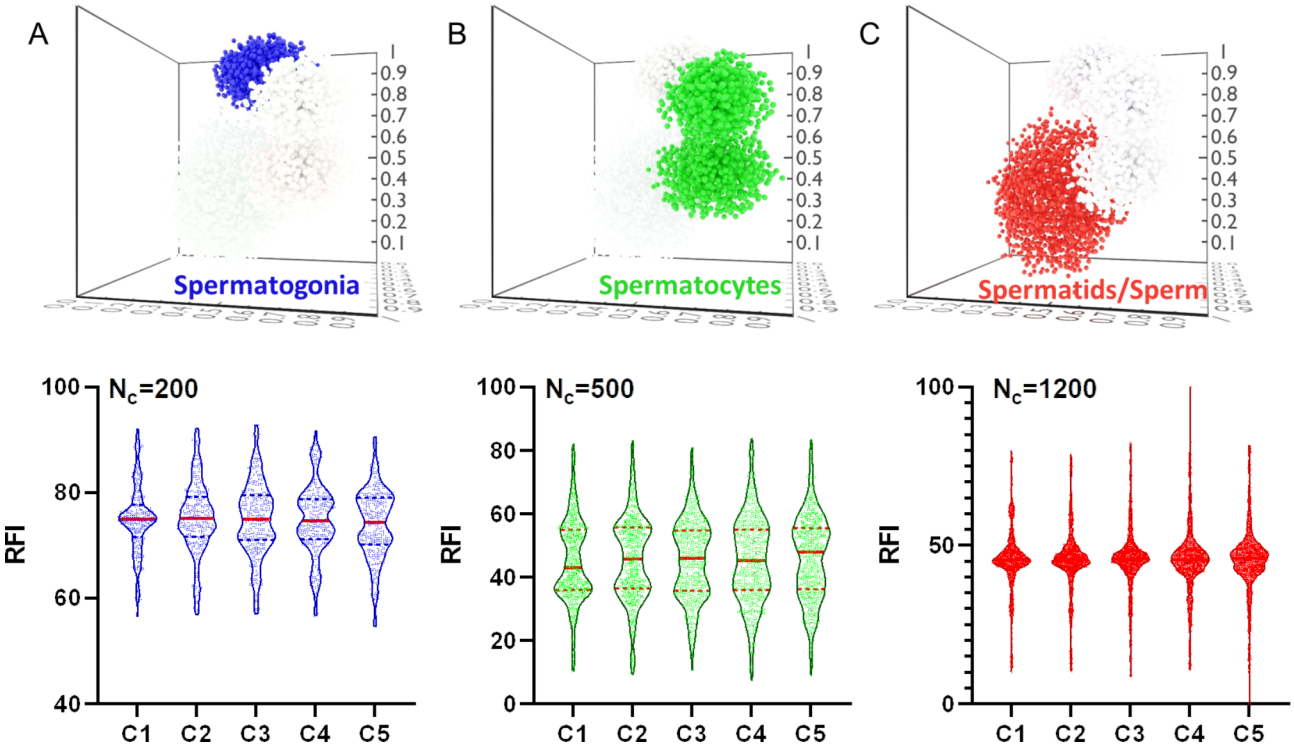

Fig. 3 Principal component and statistical analysis of the seminiferous tubule individual germ cells populations. Principal components (PC; upper row) and violin plots (bottom row) representing individual testicular/seminiferous tubule germ cell populations size, roundness/complexity and distance from lumen (PC plots x, y,z axes) and distributions of their RFI signals from H3 staining normalized per DAPI signal (violin plots). N_c – number of cells from individual populations with no observed statistically significant differences after random picking from 5 WT testicular sections (C1 – C5; tile scans; whole section life screenings). (**A**) Spermatogonial cell populations. (**B**) Spermatocyte cell populations. (**C**) Spermatid/sperm cell populations

individual nuclei (Fig. 3, lower panels) were exported for subsequent statistical analysis.

Epididymal sperm analysis

Mouse sperm preparation

Both *caudae epididymides* were dissected, and sperm from their distal regions were released into a two 200 µL droplets of M2-fertilizing medium under paraffin oil (P-LAB, Czechia) in a Petri dish and pre-tempered at 37 °C in the 5% CO2 atmosphere. After 15 min, medium with released sperm was collected into the Eppendorf tube and centrifuged for 5 min at 300 x g. Supernatant was removed and the pellet was gently resuspended in 500 µl PBS tempered to 37 °C and centrifuged again.

Sperm decondensation and immunofluorescent labelling

Sperm smeared on a glass slides were air dried for 2 h. After, the decondensing mix (0,385% DTT, 0,2% Triton X, 200 IU/ml Heparin dissolved I PBS) was applied on the heat block preheated to 37 °C for 1 min. After, decondensing solution was removed, slides were rinsed in PBS and fixed for 15 min in buffered formalin solution or 3,2% paraformaldehyde, depending on the antibody used for subsequent staining. Immuno-fluorescent staining was done using primary antibodies (Table 1) diluted 1:200 in the Antibody diluent (Zytomed Systems GmbH, Germany) and applied overnight at 4 °C. The next day, samples were washed in PBS 3×10 min at RT. Secondary antibodies (Alexa Fluor 488/568, anti-mouse/anti-rabbit secondary antibodies, Abcam, GB) were diluted 1:500 in Antibody diluent and applied in a humid chamber for 1 h. Samples were washed 3×10 min again and mounted using the Vectashield with DAPI (Vector Laboratories, USA) and sealed with nail polish. The stained decondensed mouse sperm smears were analyzed under Nikon Eclipse fluorescent microscope and/or Carl Zeiss Zeiss LSM 710 using NIS-Elements/Zen software. The consensus heat maps (Fig. 2K-M) were generated using similar approach described in [19, 20].

DNA methylation analysis

Genomic DNA isolated from testicular and epididymal sperm samples underwent bisulfite conversion and purification using the EpiTect Fast DNABisulfite Kit (Qiagen) according to the manufacturer's instructions. To quantify the methylation of single CpGs in Protamine 1(mPrm1) CpG island of the promoter region, 20 ng of bisulphate-treated DNA was amplified by PCR with specific primers.

These primers were designed to evaluate 10 CpG sites of the mPrm1 CpG island: Forward primer: AGAGG

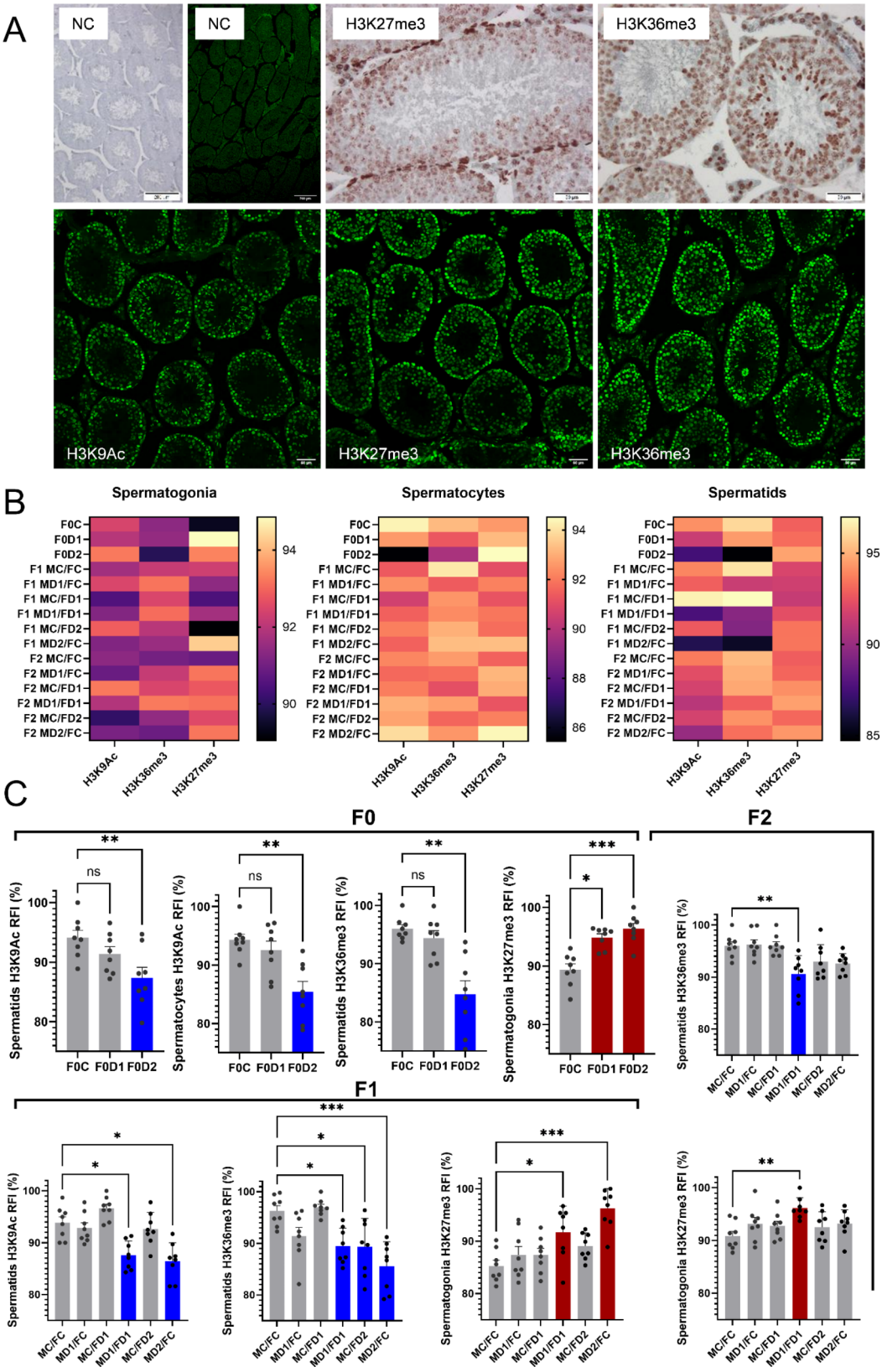

Fig. 4 (See legend on next page.)

(See figure on previous page.)

Fig. 4 Microscopic and statistical profiling of histone PTMs in testicular tissue sections (**A**) Immunohistochemical and immunofluorescent staining of testicular tissue sections. Top panel: NC – negative controls without primary antobodies/isotype for immunohistochemical staining (left) and immunofluorescent staining (right). Top and bottom panel: representative images of the testicular tissue stained with individual anti-histone PTMs antibodies – immunohistochemistry (top row) and immunofluorescent microscopy (bottom row). (**B**) Heat maps showing the differences in relative fluorescent intensities of 3 selected histone PTMs in individual testicular germ cell populations among control and experimental groups. (**C**) Inferential statistical analysis of the control and experimenal groups with detected significant differences among individual histone PTMs abundancies in individual germ cell populations in F0, F1 and F2 generation. *$p \leq 0.05$; **$p \leq 0.01$; ***$p \leq 0.001$

GTGTTGGTTTTAGGTTATAG; Reverse primer: A ACCCAACCCAACCCTCTA; Sequencing primer AT GTTGTAGTAGTAAAAGTAGGA; Target sequence GTAGATGTYGTYGTYGTAGGYGAAGATGTYG-TAGAYGGAGGAGGYGATGTTGTYGGYGGAGGAG-GYGAAGTAAGTAGAGGGTTGGGTTGGGT. The PCR reaction contained 12.5 µl of PyroMark PCR Master Mix (Qiagen, Hilden, Germany), 2.5 µl of CoralLoad (Qiagen, Hilden, Germany), and 2.5 µl of 0.2 µM primer mix, together with DNA diluted with ddH2O in to a final volume of 25 µl. The following conditions were used for PCR: 95 °C for 15 min followed by 45 cycles at 95 °C for 30 s, 56 °C for 30 s, and 72 °C for 30 s and a final extension at 72 °C for 10 min. The PCR products were pyrosequenced in Qiagen PyroMark Q24. We used the standard protocol and the required chemicals supplied by Qiagen. The received data was analyzed by Qiagen Q24 software (Version 2.0.6) (Qiagen, Hilden, Germany).

Statistical analysis

Individual numerical datasets were analyzed and plotted/graphically presented using GraphPad Prism 9 software (GraphPad Software, LLC). KW-ANOVA with subsequent Dunn's multiple comparisons test were used to analyze the significance of the differences among control and experimental groups in Figs. 4C and 5E. *$p \leq 0.05$; **$p \leq 0.01$; ***$p \leq 0.001$.

Results

Profiling of histone PTMs in testicular tissue sections

The results from the immunofluorescent staining of the testicular tissue slides showed consistent staining of all seminiferous tubules germ cell populations by western blot proven specific antibodies (anti-H3K9Ac, anti-H3K27me3 and anti-H3K36me3; Fig. 4A bottom row) with clear fluorescent signals confined to the individual cell nuclei. There was no detectable immunofluorescent signal detected in the negative control (NC with isotype controls; Fig. 4A NC left panel). In case of all three selected histone PTMs, spermatogonia nuclei showed the most intense fluorescent signal corresponding to H3 staining (Figs. 2D and 3A). In case of H3K27me3 and H3K36me3, the fluorescent intensity patterns successfully corresponded to the immuno-histochemical staining of the testicular tissue slides (Fig. 4A upper row right panels). The labelled testicular tissue section of both experimental and control animals were captured and subjected to semi-automatic in situ fluorescent analysis of the histone PTMs (Figs. 1A-I and 2). The analytical outputs delivered quantitative differences in the relative fluorescent intensity (RFI) signals in spermatogonia, spermatocytes, spermatids between control and experimental samples among for tested histone modifications (anti-H3K9Ac, anti-H3K27me3 and anti-H3K36me3) across all generations (F0, F1, F2; Fig. 4B).

In F0 generation, there was a significant decrease of the H3K9Ac RFI in spermatids ($p \leq 0.01$) and in spermatocytes ($p \leq 0.01$) of the F0D2 group compared to the F0C group. Furthermore, a significant decrease of H3K36me3 RFI in spermatids of the F0D2 group compared to the F0C group ($p \leq 0.01$) was also observed. Finally, there was a significant increase of the H3K27me3 RFI in spermatogonia in F0D1 (2.5ng/ml) and F0D2 (2.5 µg/ml) groups compared to the parental control (F0C) group (F0D1/PC $p \leq 0.05$; F0D2/PC $p \leq 0.001$; Fig. 4C P panels).

Subsequently, in F1 generation, the major differences in the histone PTMs RFI were observed in spermatids. Spermatid H3K9Ac RFI (significant decrease in MD1/FD1 and MD2/FC groups compared to MC/FC; $p \leq 0.05$), spermatid H3K36me3 RFI (significant decreases compared to control MC/FC group in MD1/FD1 group ($p \leq 0.05$), MC/FD2 group ($p \leq 0.05$) and MD2/FC group ($p \leq 0.001$). In spermatogonia the changes were observed in case of H3K27me3 (significant RFI increase compared to control group MC/FC in MD1/FD1 group ($p \leq 0.05$) and MD2/FC group ($p \leq 0.001$; Fig. 4B F1 panels).

Finally, in F2 generation the major significant differences in individual PTMs RFI were observed in spermatids in case of H3K36me3 (significant decrease in MD1/FDMC/FC group compared to MC/FC control group, $p \leq 0.01$) and in spermatogonia in case of H3K27me3 (significant increase in MD1/FD1 group compared to control; Fig. 4B F2 panels).

In general, a decrease in H3K9Ac / H3K36me3 RFI was observed particularly in spermatids across all three generations, and this was contrasted to an increase in H3K27me3 RFI in their spermatogonia. The effect of EE2 exposure was noticeable also by decrease of H3K9Ac RFI in spermatocytes of F0 generation, but this pattern was not carried to F1 or F2.

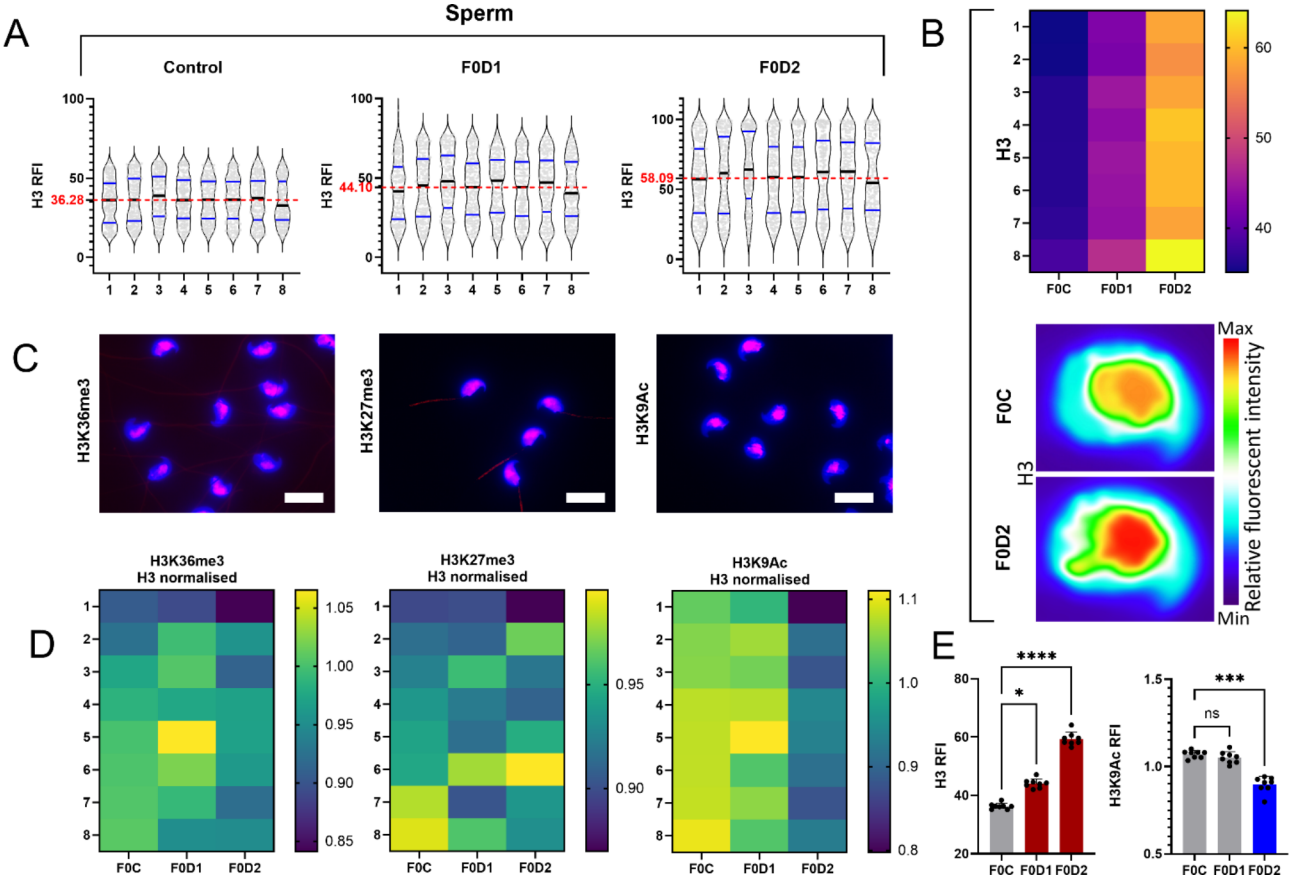

Fig. 5 Microscopic and statistical analysis of core histones and histone PTMs abundancies in sperm. (**A**) Violin plots showing the epididymal sperm sample variabilities in core H3 histone fluorescent staining among P generations - control and experimental (F0D1; F0D2) groups ($N_{samples}$ = 8; N_{cells} = 200). (**B**) Heat map represents differences in core histone H3 staining among parental control (F0C) and experimental groups ($N_{samples}$ = 8; top panel) and consensus in situ heat map of sperm nuclei H3 staining from control F0C group (bottom upper panel) and experimental F0D2 group (bottom lower panel). (**C**) Representative images showing immunofluorescent staining of individual histone PTMs in decondensed sperm nuclei. Scale bare 10 µm. (**D**) Heat maps represents H3 normalized histone PTMs sperm nuclei abundancies among control and experimental groups of P generation. (**E**) Inferential statistical analysis of the control and experimenal groups with the detected significant differences among individual core H3 histone and histone PTMs abundancies in sperm nuclei in P generation. *$p \leq 0.05$; **$p \leq 0.01$; ***$p \leq 0.001$. Red columns indicate a significant RFI increase; blue columns indicate a significant RFI decrease

Analysis of core histones and histone PTMs abundancies in sperm

Fluorescent analysis of core H3 abundancies (Fig. 2I-M) showed qualitative and quantitative differences between control and experimental epididymal sperm samples. Outputs from the analysis of control group samples showed lowest variance in H3 abundancies and corresponding H3 RFI and lowest averaged RFI (36.28) when compared to experimental F0D1 (higher variance, averaged RFI=44.10) and F0D2 group (highest variance among individual samples/animas, averaged RFI=58.09) (Fig. 5A). The in situ consensus heat map supported these findings and showed differential distribution of the H3 fluorescent signals among sperm nuclei. Importantly, the signal from F0D2 group was both quantitatively higher, and showed increased H3 persistence in the basal part of the mice sperm nuclei, specifically in the proximity of the head-to-tail coupling apparatus (Fig. 5B bottom panel). Subsequent immunofluorescent imaging of the histone PTMs showed specific nuclear staining pattern in areas corresponding to core H3 staining, particularly for anti-H3K9Ac and anti-H3K36me3 (Fig. 5C). In case of anti-H3K27me3, unspecific staining of the sperm midpiece was observed with no effect on subsequent quantitative analysis (analysis of RFI in DAPI ROI; Fig. 5C middle panel). The individual PTMs RFI were normalized per averaged core H3 RFI in individual groups to directly compare differences in PTMs RFI subtracted from observed differences in H3 RFI signals (Fig. 5D). During quantitative statistical analysis, a significant increase in core H3 RFI was detected (F0D1/F0C $p \leq 0.05$; F0D2/ F0C $p \leq 0.001$) as well as a significant decrease of H3 normalized H3K9Ac RFI in F0D2 group compared to control F0C ($p \leq 0.001$). No further significant differences were observed among sperm samples from F1 and F2 generations.

Red columns indicate a significant RFI increase; blue columns indicate a significant RFI decrease.

Analysis of protamine 1 promotor methylation status

Methylation analysis of individual CpG sites from Prm1 gene CpG island area in F0 generation between control and experimental F0D2 groups did not show statistically significant differences in the percentages of methylated mPrm1 CpG sites between F0C and F0D2 group and hence the F0D1; subsequent generations have been not analyzed. The differences were examined in testicular, epididymal and sperm samples. In the testicular tissue samples, the % of the methylated CpG sites in the F0D2 group was slightly lower 82.46±3,74 vs. 84,22±3,85 compared to control samples ($p \geq 0.05$; Fig. 6A). In both caput and corpus epididymis the similar decreasing pattern was observed while it was most prominent in the corpus epididymis 37.86±7.88 (F0C) vs. 26.32±9.88 (F0D2). Without reaching the statistical significance samples ($p \geq 0.05$; Fig. 6C). Finally, in sperm no statistically significant differences in % of methylated CpG sites were observed and both control and experimental samples showed highly similar profile of % CpG methylation 73.96±5.01 (F0C) vs.74.22±4.74 (F0D2) ($p \geq 0.05$; Fig. 6E). Outputs from all parts of the epididymis are summarized and presented as Fig. 6F.

Discussion

EE2 effect on histone PTMs in individual male germ cell types

The seminiferous epithelium within seminiferous tubules is occupied by one of the most heterogeneous cell populations among all tissue types with cells displaying distinct variety of endocrine receptors [8] and specific nuclear organization [21]. Contrary to somatic Sertoli cells, male germ cells are produced in the process of spermatogenesis and originate from spermatogonia stem cells occupying a niche at the seminiferous tubule basal

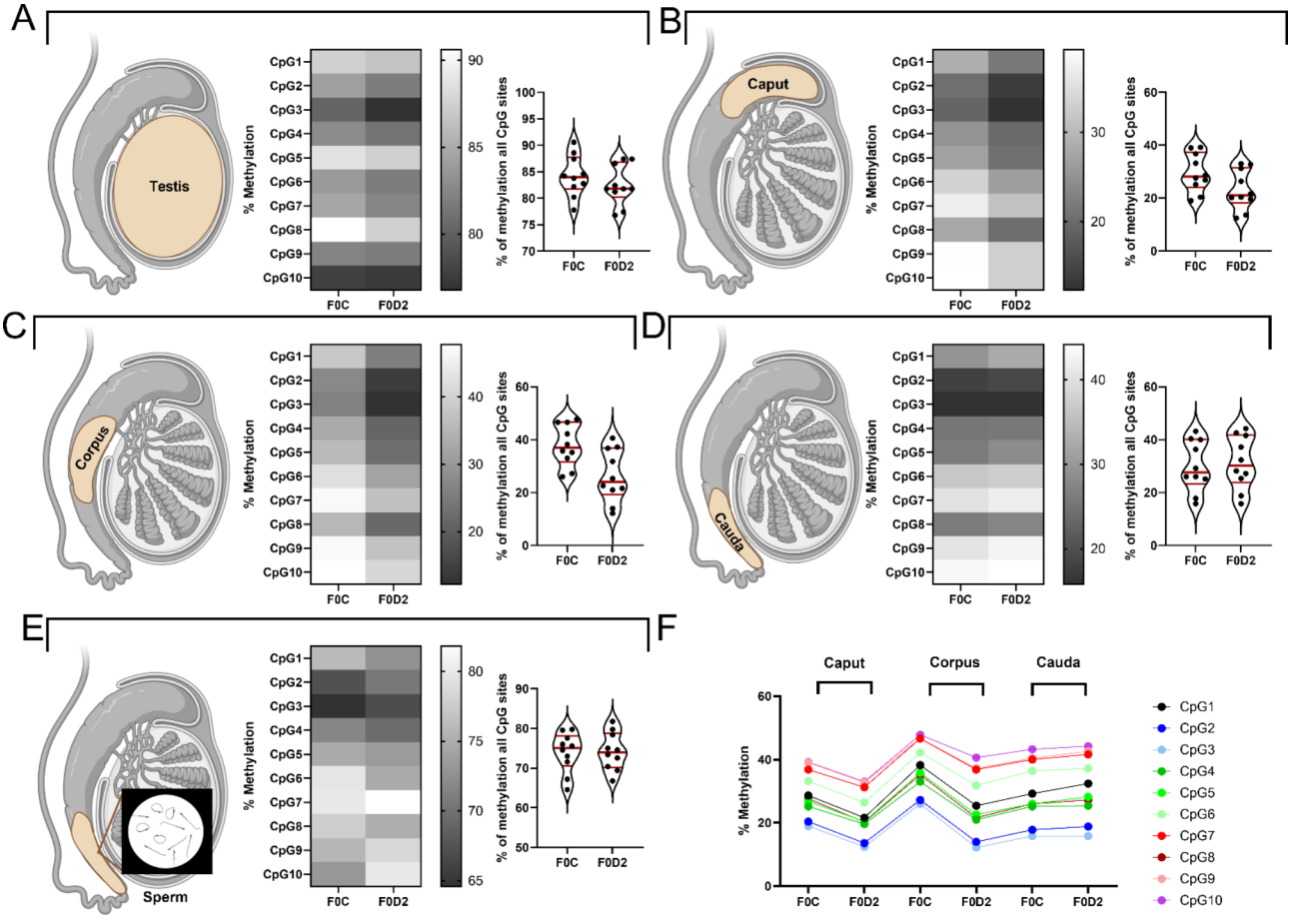

Fig. 6 Analysis of protamine 1 promotor methylation status in testis, epididymis and sperm. Methylation analysis of individual CpG sites from Prm1 gene CpG island area in the parental (F0) generation between control and experimental F0D2 groups. (**A**) Heat map showing % methylation of individual (1–10) CpG sites from testicular tissue (cartoon on the left) and the violin plots showing the total methylation status among all CpG sites (showed as data points) in F0C and experimental F0D2 groups (right). (**B**) Corresponding results for *caput epididymis*. (**C**) *Corpus epididymis*. (**D**) *Cauda epididymis*. (**E**) Epididymal sperm isolated from *cauda epididymis*. (**F**) Tendency plot showing % methylation of 1–10 Prm1 CpG sites in individual parts of epididymis (*caput*, *corpus*, *cauda*) in control (F0C) and experimental (F0D2) samples

lamina. Hence, both variability and partial propagation of the chromatin and epigenetic patterns in response to endocrine stimuli can be expected.

In spermatogonia stem cells, activation and repression of histone marks and their specific localization and tightly regulated balance are essential for their self-renewal and regular differentiation into primary spermatocytes [22] Also, the specific effect of estrogen stimuli on spermatogonia via GPR30 receptor [23] and permanent disruption of their chromatin status with the propagation to meiotic spermatocytes [24] was reported. In our study, a significant effect of EE2 was observed, specifically the increase in H3K27me3 spermatogonial nuclear histone PTMs (mark) in F0 generation (F0D1 and F0D2 groups), propagation to F1 generation in MD1/FD1; MD2/FC groups and finally in F2 generation in MD1/FD1 group. H3K27me3 histone is primarily connected to a repression of the gene expression and formation of heterochromatin domains in the cell nuclei [25]. Hence, the higher abundance of H3K27me3 in spermatogonia nuclear chromatin in response to EE2 exposure could possibly be related to the dysregulation of spermatogonial stem cell homeostasis and be potentially responsible for the lower ability of these stem cells to enter the differentiation process to generate primary spermatocytes in high level estrogen environment. Since the propagation of the EDs disruptive effect from spermatogonia to spermatocytes and to whole spermatogenesis has been reported [24], the changed H3K27me3 abundance in spermatogonia could subsequently effect chromatin structure and corresponding specific aspect of chromatin homeostasis in spermatocytes and spermatids/sperm. Here, in both cases the H3K27me3 abundance was (not significantly) higher in F0D2 groups, which may reflect the transfer of this nuclear histone pattern from spermatogonia to subsequent cell stages during spermatogenesis rather than a consequence of direct effect of EE2.

Primary and secondary spermatocytes are next subsequent stage of spermatogenesis. The major distinct cellular aspect of these cell stages is reflected by meiosis (meiosis I and II), accompanied by specific chromatin regulation events related to different histone PTMs [26]. Meiosis is a highly complex process prone to be disrupted by EDs particularly with estrogenic activity in both males [27] and females [28]. In our study, the major difference between the control and experimental groups was in a significantly lower abundance of H3K9Ac in the parental experimental (F0D2) group compared to the control (F0C). In general, histone acetylation is associated with transcriptional activation and associated with euchromatin formation [25]. H3K9Ac was both confirmed to be expressed in spermatocytes and its rapid but reversible decrease is reportedly connected to DNA damage [29]. Hence, the observed significant decrease in H3K9Ac among male germ cells of the meiotic stage could have resulted from the cellular/meiotic/DNA stress after the EE2 exposure. The (not significant) decrease in H3K36me3 could further be in context with possibly altered Prdm9 action [30] on recombination hotspots as well as with cellular/meiotic/DNA stress induced H3K9Ac decrease.

Spermiogenesis, represents critical stage with major distinct nuclear/chromatin remodeling and histone-to-protamine exchange which are major targets of EDs action in mammals. Similarly to spermatocytes, the significantly lower abundancies of H3K9Ac and H3K36me3 were observed in spermatids. Due to the fact that the histone acetylation is the major event preceding the exchange of histones to transition proteins and finally protamines, the detected decrease in H3K9Ac reflects a higher retention of histones in epididymal sperm in both F0D2 groups compared to F0C. Both H3K9Ac and H3K36me3 decrease could have also partially resulted from the same observed pattern in spermatocytes (like spermatogonia-spermatocytes transmission in H3K27me3) and may have significant impact on sperm physiology. This impact may be mediated by both changes in the nuclear shape and volume as well as changes signaling via nuclear matrix/lamina/periphery structures. Finally, the changes of epigenetic profiles in sperm nucleus may ultimately interfere with post-fertilization events and influence early embryonic development (last section of the Discussion).

Global and local effect of estrogens on chromatin remodeling

In general, endocrine function are shaped by epigenetic mechanisms, which link environmental factors with genetic regulations [31]. Environmental factors, endocrine functions and genetic/epigenetic mechanisms are interconnected in self-regulatory networks and environmental change like the exposure to EDs has specific/limited and/or global impact on both endocrine and epigenetic regulatory landscapes. In case of estrogen/EDs with estrogenic activity exposure, the most specific epigenetic effect will be on the DNA methylation/histone PTMs profile in estrogen response-elements (EREs) of estrogen-responsive genes. In our study we utilized the in situ labeling of the histone PTMs on the level of the whole nuclei section staining. Therefore, the observed changes in the RFI of signals from individual nuclei cannot result only from direct changes in ERs regions, which represent only fragment of the entire genome. The fact of measurable differences of the entire nuclei section between control and experimental groups can be explained by the fact that epigenetic reprogramming at estrogen-receptor binding sites alters 3D chromatin landscape with profound impact on the histone PTMs abundancies in the

chromatin of exposed cells [32]. Furthermore, on the tissue level, estrogens have profound impact on cell-to-cell communication and paracrine regulations in the estrogen-responsive tissues. Finally, on the organismal level, EDs with estrogenic activity interfere not only with estrogen regulations, but also with the whole endocrine system regulatory pathways, while in the testis, the anti-androgenic effect is important to mention. Hence, in our study, the observed changes in total histone PTMs abundancies in individual testicular cell types reflects EE2 in vivo effect on all above-mentioned levels of complexity. Our study therefore presents important insight into in vivo epigenetic aspects of EE2 exposure in its complexity and physiological significance. For the isolation and in-depth analysis of the individual molecular (EREs) to organismal (anti-androgenic) effect, other experimental models like cell cultures and testicular in vitro models can be used (Fig. 7).

Cumulative, multigenerational and trans-generational transmission of histone PTMs patterns

Additionally, due to the design of this study the histone/DNA methylation patterns and transmission of the histone PTMs pattern from cell to cell during spermatogenesis to subsequent generation could be addressed (Fig. 1). During fertilization, sperm and oocyte deliver their unique epigenetic profiles to the zygote, which have a profound effect/impact on the early embryonic development and entire epigenetic landscape of the progeny. In presented study, the partial multigenerational effect in F1 generation was observed in case of the individual seminiferous cell populations, when the detected differential histone PTMs abundancies mostly followed the paternal transmission (Fig. 4C F0/F1 panels). The observed differences in testicular cell populations were not transmitted to any significantly different histone PTMs abundance in epididymal sperm populations indicating possible employment of compensatory mechanisms after EE2 exposure in both studied doses. This compensatory mechanism may involve testicular tissue specific processes as well as detoxification process in liver particularly demonstrated for H3K27me3 PTMs [33]. This was further true in F2 generation, when only continuously exposed MD1/FD1 group expressed significant differences in histone PTMs abundancies including spermatogonial H3K27me3 (Fig. 4C F2 panel) when changes detected in germ cell populations were not transmitted to epididymal sperm populations. Importantly, based on our experimental set-up, there was no trans-generational effect observed for the F2 generation, which may reflect both the decline of F0 exposure effect towards the F2 generation, species specific response and ability of trans-generational recovery/reparation system, as

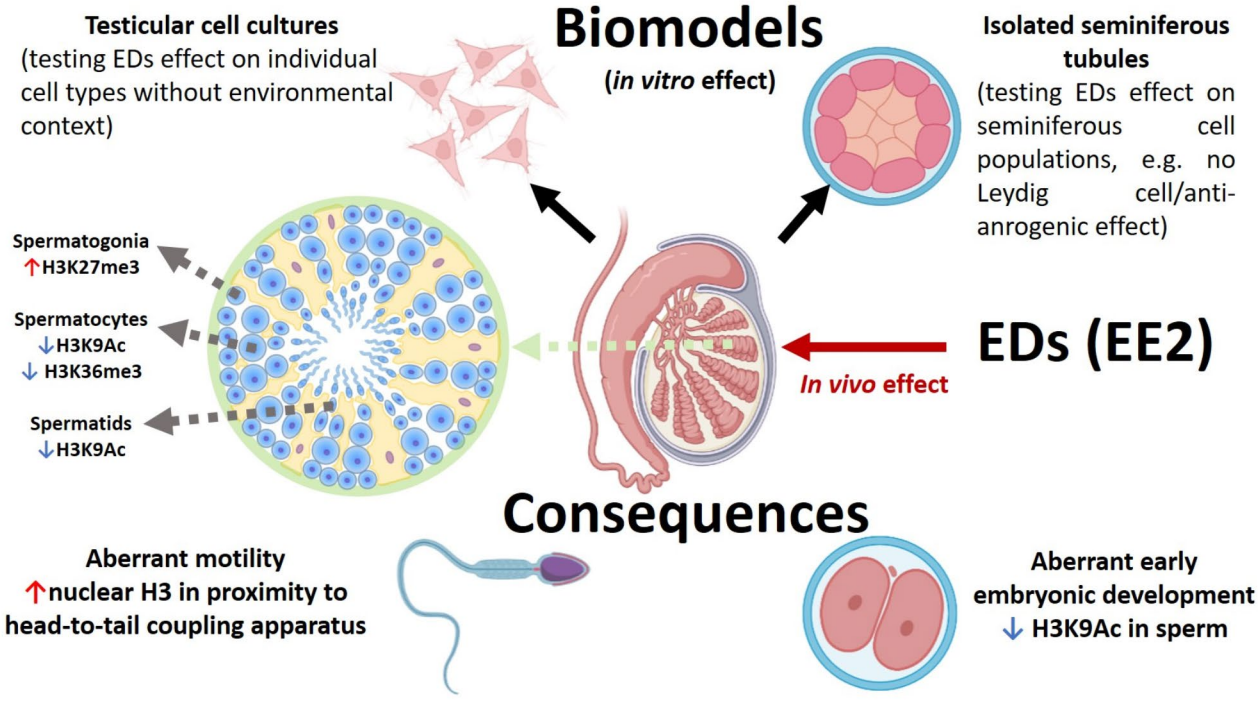

Fig. 7 Summary of major observed effects of EE2 exposure on testicular and sperm epigenetic profiles. Presented biomodels for in depth analysis of individual EE2 epigenetic mechanisms, and potential physiological consequences of observed epigenetic changes

well as the limits (sensitivity) of the performed analytical procedures.

Methodological approach and implications for sperm physiology and early embryonic development

In situ fluorescent microscopy used to assess histone PTMs profiles among individual germ cell populations in control and experimental groups requires careful normalization steps of methodological differentiation and representation of individual cell populations for subsequent statistical analysis. Therefore, the complex analytical approach was implemented (Figs. 2 and 3) to assess the statistical differences in relative fluorescent intensities between individual germ cell populations with emphasis on their sensitivity and specificity. The major methodological limitation of our approach was a selection of a limited number of histone PTMs for the analysis by monoclonal antibodies. The histone code consists of tens of specific histone PTMs and thousands of combinations of individual amino acid residues located particularly at the N-terminus [34]. The potential methodological alternative for the analysis of histone PTMs abundancies to the monoclonal antibodies is nano-liquid chromatography-tandem mass spectrometry used to assess the histone PTMs abundancies among human sperm samples [35]. Furthermore, in situ fluorescent analysis of histone PTMs rather reflect changes of global epigenetic landscape in individual cell types after EE2 (or general estrogenic/EDs) exposure, but do not provide the information about the local changes at important genomic sites. Here, the DNA methylation analysis and/or chromatin immunoprecipitation [36–38], their combination [39] and microRNA expression profiling [40] provide sequence specific information in the genomic regions of interest. On the other hand, the overall impact of the sperm nucleus increased histone retention on sperm physiology, post-fertilization pronuclear formation/fusion, and early embryonic development may reflect the core histones and their PTMs total abundancies. At the same time it may also reflect a location among higher order nuclear architecture rather than their sequence-specific genomic localization [38, 41]. Therefore, the discovery and quantitative representation of the increased histone retention in the basal part of the sperm nucleus is critical output of this study (Fig. 5B lower panel). The histone retention is represented by consensus heat map and possibly represents a direct impact of EE2 exposure on the sperm nuclear architecture. Consequently, the sperm motility could be altered by the propagation of the change to the head-to-tail coupling apparatus as a result of insufficient histone-protamine exchange (Fig. 7).

Supplementary Information

The online version contains supplementary material available at https://doi.org/10.1186/s12958-024-01307-6.

Supplementary Material 1

Supplementary Material 2

Acknowledgements

We acknowledge Imaging Methods Core Facility at BIOCEV supported by the MEYS CR Large RI Project and Czech-BioImaging, and MFF Imaging Core Facility supported by ZEISS Group, for their support with obtaining imaging data presented in this paper. We are thankful to TUM Language Editing Services for English corrections.

Author contributions

LD – study design, manuscript writing, data acquisition, data analysis, grant acquisition; EZL – laboratory work; EV - laboratory work, data acquisition and curation; MF - laboratory work, data acquisition and curation; OSa - laboratory work, data acquisition and curation; VP - laboratory work, mouse colony management, data acquisition and curation; OSi - laboratory work, data acquisition and curation; AD - laboratory work, data acquisition and curation; HM - laboratory work; FE – animal handling and exposure, laboratory work; AK – laboratory work and sperm handling; JP – supervision, advisory input to mouse study design; APD – study design, data acquisition, analysis and curation; KS – study design, project cooperation management, grant acquisition; KK – study design, supervision, financial acquisition, manuscript writing. All authors read and approved the manuscript.

Funding

The study was funded by the Czech Science Foundation (GACR Nos. GJ20-17403Y and GA23-06591S) to LD; the Institute of Biotechnology RVO (86652036); BIOCEV project (CZ.1.05/1.1.00/02.0109) from the ERDF; MEYS CR Large RI Project (LM2018129); COST Action CA20119 (ANDRONET) supported by European Cooperation in Science and Technology (www.cost.eu); Czech-BioImaging (CZ.02.1.01/0.0/0.0/16_013/0001775) and (CZ.02.1.01/0.0/0.0/18_046/0016045); and DFG STE 892/20 – 1 to KS.

Data availability

Exact PCA coordinates for semi-automatic segmentation related to Fig. 2H / Fig. 3 upper panels is attached as Supplementary file 1. Primary numerical data for RFIs of individual segmented testicular cell populations types related to Fig. 3 lower panels is attached as Supplementary file 2.

Declarations

Ethics approval

The experimental protocol of the mice in vivo study was approved by the Animal Care and Use Committee of the Institute of Molecular Genetics ASCR and carried out in accordance with the regular relevant guidelines and regulations (file number 17OZ9715/2019–18134).

Consent for publication

Not applicable.

Competing interests

The authors declare no competing interests.

Received: 25 October 2023 / Accepted: 23 October 2024
Published online: 04 November 2024

References

1. *Knobil and Neill's Physiology of Reproduction, Vols 1 and 2, 3rd Editon*. Knobil and Neill's Physiology of Reproduction, Vols 1 and 2, 3rd Editon, 2006: pp. 1-3238.
2. Bao J, Bedford MT. Epigenetic regulation of the histone-to-protamine transition during spermiogenesis. Reproduction. 2016;151(5):R55–70.

3. Ded L, et al. Effect of estrogens on boar sperm capacitation in vitro. Reprod Biol Endocrinol. 2010;8:87.
4. Ded L, et al. In vivo exposure to 17beta-estradiol triggers premature sperm capacitation in cauda epididymis. Reproduction. 2013;145(3):255–63.
5. Sebkova N, et al. The slower the better: how sperm capacitation and acrosome reaction is modified in the presence of estrogens. Reproduction. 2012;143(3):297–307.
6. Eddy EM, et al. Targeted disruption of the estrogen receptor gene in male mice causes alteration of spermatogenesis and infertility. Endocrinology. 1996;137(11):4796–805.
7. Dumasia K, et al. Estrogen, through estrogen receptor 1, regulates histone modifications and chromatin remodeling during spermatogenesis in adult rats. Epigenetics. 2017;12(11):953–63.
8. Dostalova P, Zatecka E, Dvorakova-Hortova K. Of Oestrogens and sperm: a review of the roles of oestrogens and oestrogen receptors in male reproduction. Int J Mol Sci. 2017;18(5).
9. Kabir ER, Rahman MS, Rahman I. A review on endocrine disruptors and their possible impacts on human health. Environ Toxicol Pharmacol. 2015;40(1):241–58.
10. Rowan JP, et al. Effects of low-dose norethindrone acetate plus ethinyl estradiol (0.5 mg/2.5 microg) in women with postmenopausal symptoms: updated analysis of three randomized, controlled trials. Clin Ther. 2006;28(6):921–32.
11. Coelingh Bennink HJ, et al. The use of high-dose estrogens for the treatment of breast cancer. Maturitas. 2017;95:11–23.
12. Kuhl H. Pharmacology of estrogens and progestogens: influence of different routes of administration. Climacteric. 2005;8(Suppl 1):3–63.
13. Kidd KA, et al. Collapse of a fish population after exposure to a synthetic estrogen. Proc Natl Acad Sci U S A. 2007;104(21):8897–901.
14. Morteani G, et al. Input and fate of anthropogenic estrogens and gadolinium in surface water and sewage plants in the hydrological basin of Prague (Czech Republic). Environ Geochem Health. 2006;28(3):257–64.
15. Brehm E, Flaws JA. Transgenerational effects of endocrine-disrupting chemicals on male and female reproduction. Endocrinology. 2019;160(6):1421–35.
16. Dupont C, Armant DR, Brenner CA. Epigenetics: definition, mechanisms and clinical perspective. Semin Reprod Med. 2009;27(5):351–7.
17. Van Cauwenbergh O, et al. Transgenerational epigenetic effects from male exposure to endocrine-disrupting compounds: a systematic review on research in mammals. Clin Epigenetics. 2020;12(1):65.
18. Brieno-Enriquez MA, et al. Exposure to endocrine disruptor induces transgenerational epigenetic deregulation of microRNAs in primordial germ cells. PLoS ONE. 2015;10(4):e0124296.
19. Schneider S et al. Protamine-2 deficiency initiates a reactive oxygen species (ROS)-mediated destruction cascade during epididymal sperm maturation in mice. Cells. 2020;9(8).
20. Merges GE et al. Loss of Prm1 leads to defective chromatin protamination, impaired PRM2 processing, reduced sperm motility and subfertility in male mice. Development. 2022;149(12).
21. Meikar O, Ros MD, Kotaja N. Epigenetic regulation of male germ cell differentiation. Subcell Biochem. 2013;61:119–38.
22. Wu H, Sun YE. Epigenetic regulation of stem cell differentiation. Pediatr Res. 2006;59(4 Pt 2):21R-5R.
23. Sirianni R, et al. The novel estrogen receptor, G protein-coupled receptor 30, mediates the proliferative effects induced by 17beta-estradiol on mouse spermatogonial GC-1 cell line. Endocrinology. 2008;149(10):5043–51.
24. Vrooman LA, et al. Estrogenic exposure alters the spermatogonial stem cells in the developing testis, permanently reducing crossover levels in the adult. PLoS Genet. 2015;11(1):e1004949.
25. Kouzarides T. Chromatin modifications and their function. Cell. 2007;128(4):693–705.
26. Wang LN, et al. The histone codes for meiosis. Reproduction. 2017;154(3):R65–79.
27. Liu C, et al. Exposure to bisphenol a disrupts meiotic progression during spermatogenesis in adult rats through estrogen-like activity. Cell Death & Disease. 2013:4.
28. Brieno-Enriquez MA, et al. Human meiotic progression and recombination are affected by Bisphenol A exposure during in vitro human oocyte development. Hum Reprod. 2011;26(10):2807–18.
29. Tjeertes JV, Miller KM, Jackson SP. Screen for DNA-damage-responsive histone modifications identifies H3K9Ac and H3K56Ac in human cells. EMBO J. 2009;28(13):1878–89.
30. Powers NR et al. The meiotic recombination activator PRDM9 trimethylates both H3K36 and H3K4 at recombination hotspots in vivo. PLoS Genet. 2016;12(6).
31. Zhang XA, Ho SM. Epigenetics meets endocrinology. J Mol Endocrinol. 2011;46(1):R11–32.
32. Achinger-Kawecka J et al. Epigenetic reprogramming at estrogen-receptor binding sites alters 3D chromatin landscape in endocrine-resistant breast cancer. Nat Commun. 2020;11(1).
33. Wang S, et al. Epigenetic compensation promotes liver regeneration. Dev Cell. 2019;50(1):43–e566.
34. Wang ZB, et al. Combinatorial patterns of histone acetylations and methylations in the human genome. Nat Genet. 2008;40(7):897–903.
35. Schon SB, et al. Histone modification signatures in human sperm distinguish clinical abnormalities. J Assist Reprod Genet. 2019;36(2):267–75.
36. Yamaguchi K, et al. Re-evaluating the localization of sperm-retained histones revealed the modification-dependent accumulation in specific genome regions. Cell Rep. 2018;23(13):3920–32.
37. de la Iglesia A, et al. Insights into the sperm chromatin and implications for male infertility from a protein perspective. Wires Mechanisms of Disease; 2022.
38. Paradowska A, et al. Genome wide identification of promoter binding sites for H4K12ac in human sperm and its relevance for early embryonic development. Epigenetics. 2012;7(9):1057–70.
39. Pardowska-Dogan A, et al. DNA methylation analysis of histone h4k12ac associated promoters in sperm of healthy donors and subfertile patients. J Urol. 2014;191(4):E743–4.
40. Brieno-Enriquez MA et al. Exposure to endocrine disruptor induces transgenerational epigenetic deregulation of MicroRNAs in primordial germ cells. PLoS ONE. 2015;10(4).
41. Sakamoto M et al. Paternally inherited H3K27me3 affects chromatin accessibility in mouse embryos produced by round spermatid injection. Development. 2022;149(18).

Publisher's note